Seedless Velocimetry Measurements by Schlieren Image Velocimetry

Michael J. Hargather,* Michael J. Lawson,† and Gary S. Settles‡
Pennsylvania State University, University Park, Pennsylvania 16802
and
Leonard M. Weinstein§
National Institute of Aerospace, Hampton, Virginia 23666

Schlieren optical systems have been used to perform velocity measurements in refractive turbulent flows using particle image velocimetry algorithms. This schlieren image velocimetry (schlieren "particle image velocimetry") technique makes use of naturally occurring refractive turbulent eddies in a flow as virtual "seed particles" upon which velocimetry is performed. Current experiments are performed in a supersonic wind tunnel to measure the Mach 3 turbulent boundary-layer mean velocity profile. Results from schlieren, shadowgraph, and focusing schlieren image velocimetry are compared with the boundary-layer velocity profile derived from a pitot-pressure survey. Focusing schlieren optics allow the visualization of refractive disturbances within a limited depth of focus, resulting in seedless velocimetry within a narrower depth of field. The natural intermittency of the turbulent boundary layer complicates schlieren image velocimetry, but useful measurements are still possible. The velocity profile in a subsonic turbulent boundary layer is also measured using this technique through thermal seeding of the boundary layer to provide refractive turbulent structures for velocimetry. An important improvement in schlieren image velocimetry, the use of a pulsed light-emitting-diode light source in place of the twin pulsed lasers required for traditional particle image velocimetry measurements, is introduced. This comparatively inexpensive white-light source eliminates traditional problems of coherent laser illumination in schlieren imaging and improves the overall results.

Nomenclature

A	=	aperture diameter
a	=	unobstructed height of light-source image in cutoff plane
L	=	length from schlieren lens to source grid
L'	=	length from schlieren lens to cutoff grid
l	=	length from schlieren lens to plane of focus
l'	=	length from schlieren lens to image plane
U_∞	=	freestream velocity
u	=	local flow velocity
y	=	distance perpendicular to wind-tunnel floor
γ	=	intermittency function
δ	=	boundary-layer thickness
ϵ	=	refraction angle (arcseconds)
ζ	=	intermittency function parameter
σ	=	standard deviation

*Senior Research Associate, Department of Mechanical and Nuclear Engineering, Gas Dynamics Laboratory, 208 Reber Building. Member AIAA.

†Graduate Research Assistant, Department of Mechanical and Nuclear Engineering, Gas Dynamics Laboratory, 301D Reber Building. Member AIAA.

‡Distinguished Professor of Mechanical Engineering, Department of Mechanical and Nuclear Engineering, Director of Gas Dynamics Laboratory, 301D Reber Building. Associate Fellow AIAA.

§Senior Research Fellow, National Institute of Aerospace, 100 Exploration Way. Associate Fellow AIAA.

I. Introduction

PARTICLE image velocimetry (PIV) is a well-known and widely used technique for measuring planar velocity distributions in a range of fluid-dynamic systems. Typically, particles suspended in the moving fluid are tracked using a series of digital image pairs in order to determine local flow velocities [1]. Situations arise, however, where the use of tracer particles is impractical or impossible; thus, traditional PIV cannot be used. This has given rise to current interest in seedless velocimetry, in which something other than solid particles is tracked. One experimental method that can be used in some of these situations is schlieren image velocimetry. This technique was initially developed as schlieren PIV [2], but is renamed here to highlight its importance as a standalone technique with a range of applications.

Schlieren image velocimetry (SIV) is the technique of combining PIV equipment and software with schlieren optics for the purpose of seedless-velocimetry measurements in refractive turbulent flows. Turbulent flows are naturally seeded by eddies of various scales that travel at the local convective speed of the flow. Velocimetry can thus be performed without the need for particulate seeding, by correlating eddy motion between two consecutive schlieren or shadowgraph images. However, this approach relies upon both turbulence and refractive-index gradients in the flow, thus limiting its range of applicability. Nonetheless it naturally lends itself to high-Reynolds-number compressible flows, where both these conditions are usually met. Low-speed turbulent flows can also be measured this way if a refractive thermal or species difference is imposed.

Schlieren velocimetry was first proposed by Townend [3], but it proved impractical in the precomputer age. Papamoschou [4,5] revisited the technique, using a pattern-matching algorithm to track eddy motion in supersonic shear layers. Fu and Wu [6] used schlieren images and image-analysis software to measure velocity distributions in gas fires and explosions. The schlieren PIV technique was substantially improved by Jonassen et al. [2] using a commercially available PIV system to measure seedless velocity profiles in a helium jet in air and a supersonic turbulent boundary layer.

One observed disadvantage in prior schlieren image velocimetry studies is the integrating property of schlieren optics along the optical path [7]. The eddy motion recorded in the two consecutive images includes all motion across the entire flowfield, thus yielding a path-averaged measurement of the convective eddy speed. Thus, near-planar velocimetry is not possible using schlieren optics, as it is in traditional particle PIV with laser-sheet illumination. This limits the utility of schlieren image velocimetry in three-dimensional flows.

To attempt measurements with a restricted depth of focus, focusing schlieren optics are required. The lens-and-grid schlieren method, originally proposed by Schardin [8] in order to achieve a large field of view inexpensively, naturally also has a limited depth of focus for refractive disturbances. This technique, recently perfected by Weinstein [9], images refractive disturbances within a limited depth of focus, while disturbances outside this region are too blurred to register in the image [7]. Alvi et al. [10] combined this focusing schlieren approach with an optical deflectometer to perform point-wise measurements of turbulence within a low-speed axisymmetric jet. Garg and Settles [11] extended this pointwise approach to measurements of a supersonic turbulent boundary layer.

The present work develops further schlieren image velocimetry for the seedless velocimetry of subsonic and supersonic turbulent boundary layers. The velocity profile in a two-dimensional turbulent boundary layer provides a well-known flow on which SIV can be benchmarked and evaluated. Measurements obtained from schlieren, shadowgraph, and focusing schlieren optical systems are discussed.

II. Experimental Methods

The experimental methods required for this effort include two wind-tunnel facilities, an array of schlieren optical systems, a pulsed light-emitting-diode (LED) light source that provides the necessary PIV-type illumination, commercial PIV hardware and software.

A. Wind-Tunnel Facilities

1. Supersonic Wind-Tunnel Facility

Experiments were performed in the Pennsylvania State University Gas Dynamics Laboratory's (PSGDL) supersonic wind-tunnel facility. This is an intermittent blowdown facility with a test-section size of $0.15 \times 0.165 \times 0.60$ m. A 57 m^3, 2 MPa pressure reservoir provides a test duration of about 30 s every 20 min. The facility has a continuously variable Mach number capability over the range of Mach 1.5 to 4.0 by way of an asymmetric sliding-block nozzle.

All measurements reported here were made at a freestream Mach number of 3 with a nominal stagnation pressure and temperature of

6.9×10^5 Pa and 287 K, respectively. The boundary layer measured here was on the wind-tunnel test-section floor, as shown schematically in Fig. 1a. This boundary layer develops in a streamwise pressure gradient along the curved lower wall of the long asymmetric nozzle; thus, it is not expected to be identical to a flat-plate boundary layer. However, it has been shown to be two-dimensional in the mean.

A boundary-layer pitot-pressure survey performed at Mach 2.8 by Garg and Settles [11] was used as the benchmark for current schlieren velocimetry measurements. (Only a negligible boundary-layer change is expected between Mach 2.8 and 3 [12].) The wind-tunnel walls were approximately adiabatic, and the freestream turbulence level was on the order of 1–2%. Boundary-layer parameters, as previously determined from pitot-pressure surveys assuming constant total temperature across the boundary layer and an adiabatic wall [11], were $\delta = 25$ mm, $\delta^* = 8.35$ mm, $\theta = 1.57$ mm, $c_f = 0.0010$, $T_0 = 287$ K, $U_\infty = 608$ m/s, and a unit Reynolds number of $(52 \times 10^6)/$m.

Limited schlieren PIV boundary-layer measurements were also performed at freestream Mach numbers of 2 and 2.5. These showed that, as expected, the schlieren results are strongly dependent on the freestream density level. At Mach 2 the freestream density is twice as large as at Mach 3, and the focusing schlieren images showed better definition of the turbulent structures. However, only the results obtained at Mach 3 are considered here.

2. Subsonic Wind-Tunnel Facility

Experiments were also performed in the PSGDL subsonic wind-tunnel facility. This continuous open-circuit facility has a test-section size of $0.47 \times 0.31 \times 3.1$ m and a variable freestream velocity from 0.1 to 27 m/s. All present measurements were performed with a freestream velocity of 27 m/s. The test section has clear acrylic plastic sidewalls providing complete optical access. With schlieren visualization, some optical distortions are observed within these sidewalls, but their effect on the final schlieren images was minimized through the image processing as described later in Sec. II.D.

To allow schlieren visualization, the tunnel-floor boundary layer was thermally seeded using two thin-film-foil heaters located at the beginning of the test section, immediately after the inlet contraction. The heaters (part number KH-4085 from Omega Engineering), which spanned the test-section width and had a 0.1 m streamwise length, were maintained at a surface temperature of approximately 358 K, with approximately 7.75 kW/m^2 heat flux. As shown in Fig. 1, the boundary-layer measurements were performed at a
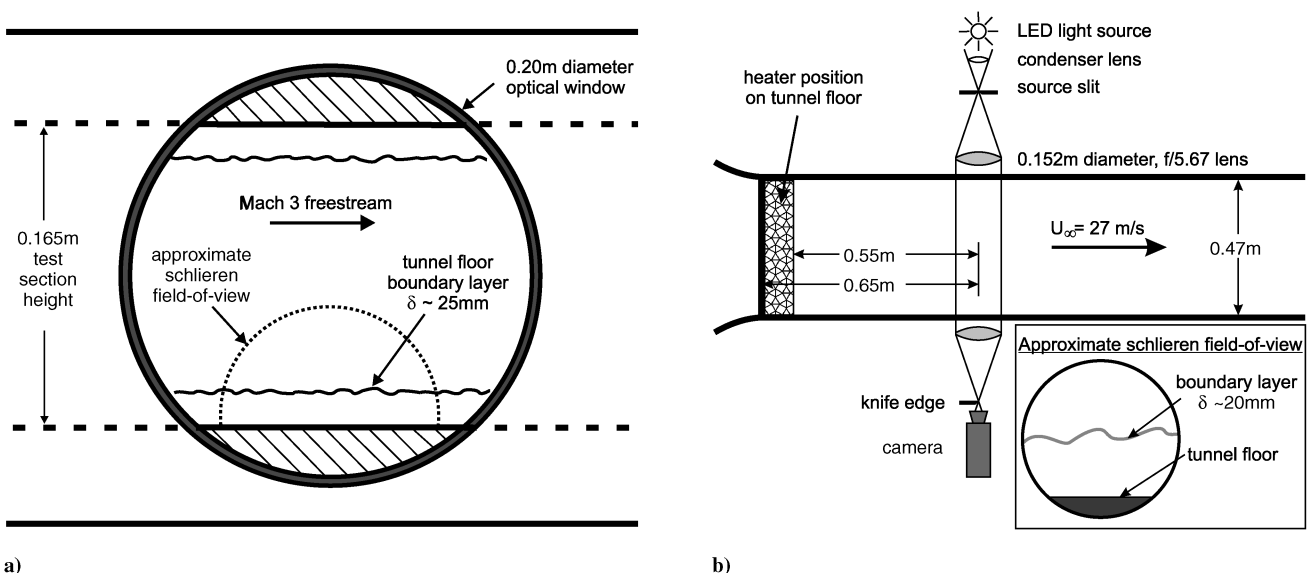

a)

b)

Fig. 1   Schematics of a) supersonic wind-tunnel test section and the approximate area being imaged and b) top view of the subsonic wind-tunnel experimental setup, including the lens-type schlieren system used for both subsonic and supersonic schlieren and shadowgraph imaging.

distance of 0.65 m downstream of the beginning of the test section (0.55 m from the end of the heaters). For comparison purposes, the boundary-layer velocity profile with thermal seeding was measured using a pitot probe.

B. Schlieren Optical Systems

Two primary optical systems are used here to image the turbulent boundary-layer structures. A focusing schlieren system is used to image turbulent structures within a limited depth of field. Traditional parallel-light (nonfocusing) schlieren optics are also used for these two-dimensional flows to obtain data for comparison with the focusing schlieren optics. However, for the subsonic boundary-layer measurements, only the parallel-light schlieren system was used.

1. Focusing Schlieren Optical System

Using the approach proposed by Weinstein [9], a focusing schlieren system was designed to image the present Mach 3 compressible turbulent boundary layer. The basics of the lens-and-grid schlieren method used here are described by Settles [7]. A schematic of the focusing optical system is given in Fig. 2. The optical components include a 0.28×0.28 m, 0.46 m focal length Fresnel lens and an 80-mm-aperture $f3.8$ schlieren field lens, along with complementary light-source and cutoff grids. The source grid is an array of horizontal clear and opaque bands that function as multiple schlieren light sources at various angles with the optical centerline. The clear and opaque bands of the cutoff grid are both 1.3 mm wide, providing approximately four opaque bands per centimeter. The cutoff grid is a photographic negative of the source grid and is located in a plane optically conjugate to it. By adjusting the cutoff grid to block a fraction of the light from reaching the image plane, the schlieren effect is achieved.

The distances between critical components of the focusing schlieren system are indicated in Fig. 2. The Fresnel lens is positioned adjacent to the source grid, with about a 2 cm spacing. The light source is positioned so as to evenly illuminate the source grid and to project a light beam via the Fresnel lens into the aperture of the schlieren field lens. The camera position is flexible depending upon the lens with which it is fitted and the field of view required for the visualization. Further information on the detailed design and construction of focusing schlieren systems is available elsewhere [7,9].

Because of the convergence of the schlieren light-beam between the source grid and the schlieren lens, the narrow region of focus is reconstructed in the vicinity of an optically conjugate plane, designated the image plane, as illustrated in Fig. 2. The limited depth of focus inside the wind-tunnel test section is defined by Weinstein [9] as the region beyond which a predetermined-length-scale structure is effectively blurred due to being out of focus. This so-called unsharp depth of focus is proportional to the distance l and inversely proportional to the aperture of the schlieren lens, A:

$$\text{depth of focus} \propto \frac{l}{A} \qquad (1)$$

The sensitivity ϵ of a lens-and-grid schlieren system is defined by Settles [7] as

$$\epsilon \propto \frac{aL}{L'(L-l)} \qquad (2)$$

where a here represents the minimum practical unobstructed height of a source-grid band image in the schlieren cutoff plane and ϵ is the minimum detectable refraction angle within the region of focus.

Equations (1) and (2) demonstrate that the depth of focus and the schlieren sensitivity are coupled. In general, schlieren sensitivity is a direct function of the strength of refractive-index gradients within the region of focus. However, for a given refractive disturbance, as the depth of focus narrows toward zero, the schlieren sensitivity likewise decreases toward zero. Thus, a practical focusing schlieren system must maintain a finite depth of focus that can never be narrowed to a true plane.

Given this tradeoff, higher schlieren sensitivity is sometimes preferable to a narrower depth of focus. One potential way to improve the schlieren sensitivity as well as the image illumination is to remove the ground glass in the image plane in Fig. 2 and project the light beam directly into the PIV camera lens. This approach, however, increases the system depth of focus by reducing its effective aperture, A, due to the small aperture of the camera lens, α. The effective depth of focus of the system is increased by the ratio of the schlieren lens aperture to the camera lens aperture: A/α.

To avoid this issue but still maintain high image illumination, one can remove the PIV camera lens and position the camera sensor at the image-plane location in Fig. 2. This technique forms the focused-schlieren image directly on the camera sensor, thus retaining the same depth of focus as with a ground-glass screen in the image plane. However, this requires a camera sensor significantly larger than those found in most or all currently available PIV cameras.

A ground-glass screen in the image plane of Fig. 2 leads to a significant loss of schlieren illumination due to light scattering, as well as some resolution loss. This problem can be addressed in part by replacing the ground glass with a screen that scatters less light (such as a holographic rear-projection screen), or by imaging directly onto the camera sensor, as stated above. Unfortunately, the present optical system does not have sufficient illumination or camera-sensor size to allow either of these solutions. Instead, the image-plane ground-glass was removed and the schlieren beam was projected directly into the camera lens by way of a 0.1 m diameter, 0.3 m focal length simple double-convex lens placed after the cutoff grid, as shown in Fig. 3. We have thus accepted the concomitant loss of depth of focus in favor of image illumination for the present experiments. Future investigations with a larger LED array are expected to improve illumination enough to permit the formation of a real image on a screen in the image plane, thus yielding a better depth of focus.
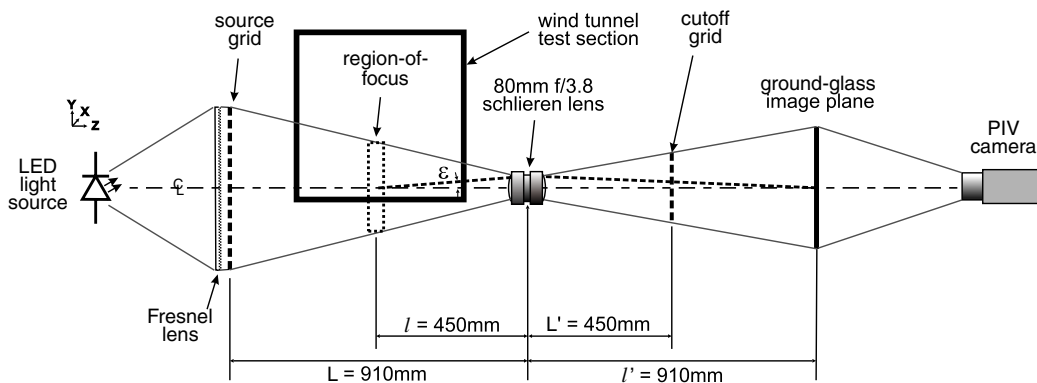

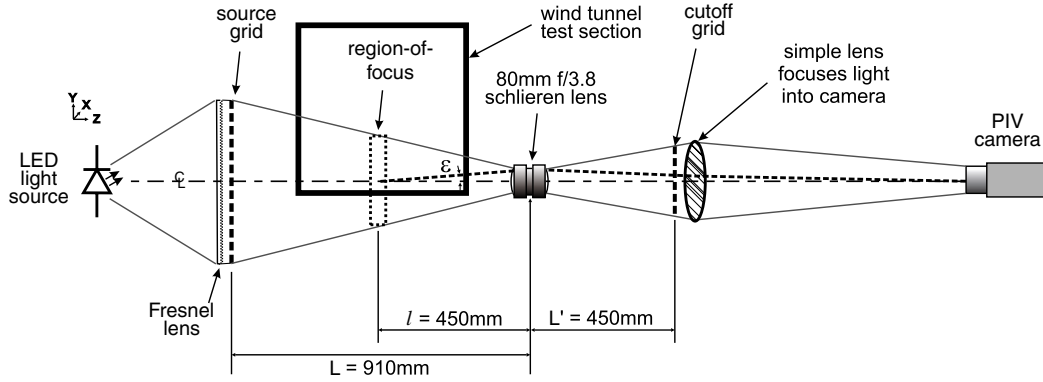**Fig. 2 Schematic of the focusing schlieren optical system.**

Fig. 3   Schematic of the final focusing schlieren optical system with a simple lens used to focus the schlieren beam into the camera.
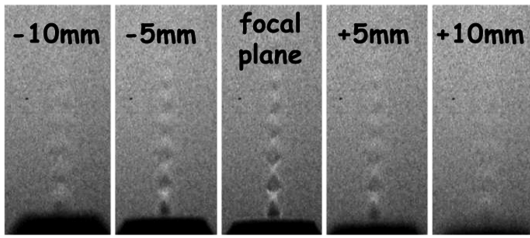

Fig. 4   Demonstration of the depth of focus for the focusing schlieren system with a ground-glass image plane, as shown in Fig. 2.

The depth of focus of the present system was experimentally determined using a 1-mm-diam underexpanded supersonic air jet. In the plane of best focus, the shock diamonds in this jet are clearly seen, as shown in Fig. 4. The jet was then traversed in 1 mm increments along the optical axis away from the plane of best focus until the shock diamonds were no longer distinguishable from the background, thus defining the unsharp depth of focus. Figure 4 shows that the present system has a depth of focus of about ± 10 mm when a ground-glass screen is present in the image plane. However, the depth of focus increased to about ± 40 mm with the screen removed and replaced by the simple lens, as in Fig. 3, which was the case for all present velocimetry experiments.

2.   Parallel-Light Schlieren and Shadowgraph Visualization

A parallel-light schlieren system featuring two 152-mm-diam $f5.67$ telescope objective lenses (Fig. 1b) was used here to image both the supersonic and subsonic boundary layers. Illumination was provided by a single 5 mm white LED, pulsed in the manner described in Sec. II.C. The same system also provided focused shadowgraph visualization, which is shadowgraphy performed with a parallel-light schlieren optical system but no knife edge cutoff [7]. The focused shadowgraphy was performed here with the PIV camera focused at about a 20 cm offset from the wind-tunnel centerline in order to provide sufficient shadowgraph sensitivity.

The purpose of these experiments was to compare the focusing schlieren results to results obtained from conventional parallel-light schlieren optics that integrate refractive effects across the entire wind-tunnel test section, including sidewall boundary layers. (Note that Jonassen et al. [2] have shown that the schlieren and shadowgraph techniques produce very similar results when used for seedless PIV of turbulent refractive flows.) The supersonic wind-tunnel test-section width is approximately 6 times the thickness of the tunnel-floor boundary layer; thus, the mean flow can be regarded as two-dimensional, and a useful comparison between focusing and integrating optics can be made.

Figure 5a shows a focusing schlieren image, and Fig. 5b shows a focused shadowgraph boundary-layer image of the supersonic boundary layer; both images have the same scale and field of view and have been processed as discussed later in Sec. II.D. Figure 5c is a schlieren image of the subsonic boundary layer, with a horizontal-knife-edge cutoff, after image processing.

The shadowgraph image (Fig. 5b) reveals finer-scale turbulence than the focusing schlieren image (Fig. 5a), which improves correlations obtained with the PIV software. The shadowgraph image also shows turbulent structures throughout the field of view, even outside the tunnel-floor boundary layer, as a result of the sidewall boundary layers on the glass windows.

The schlieren image of the subsonic boundary layer (Fig. 5c) shows a clear definition of the boundary-layer edge, because only the boundary layer has been thermally seeded, not the freestream. The sidewall boundary layers and any freestream turbulence are thus not evident, because there are no other refractive disturbances in this incompressible flow.

C.   LED Light Source

Early experiments with these optical systems used a dual-head Nd: YAG laser as the light source [2], but significant problems with coherent artifact noise and other laser-related issues, especially with the focusing schlieren optics, led us to explore the development of an alternative white-light source. (Laser illumination is needed to produce a light-sheet in traditional PIV, but not here.)

To be effective for velocimetry of high-speed flows, the SIV light source must produce two bright illumination pulses with pulse widths and interval between pulses in the microsecond range. Prior work [2] showed that xenon flashlamps cannot generally meet this requirement, because their illumination quenches too slowly after the
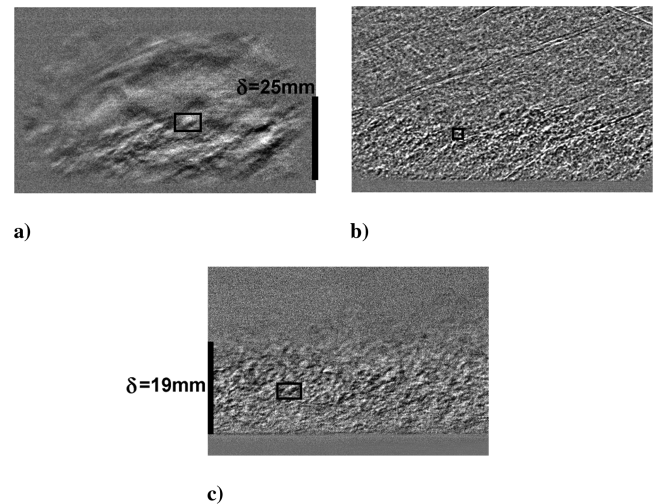

Fig. 5   Images of tunnel-floor boundary layers: a) focusing schlieren image of $M = 3$ boundary layer, b) focused shadowgraph of $M = 3$ boundary layer, and c) parallel-light schlieren image of thermally seeded subsonic boundary layer. The scale in each image shows the height of the boundary-layer edge, measured from the tunnel floor, which is at the base of the vertical scale mark. The interrogation window for each image series is also shown in each image as a rectangular box. The interrogation-window sizes are selected to fully encompass a typical turbulent structure.
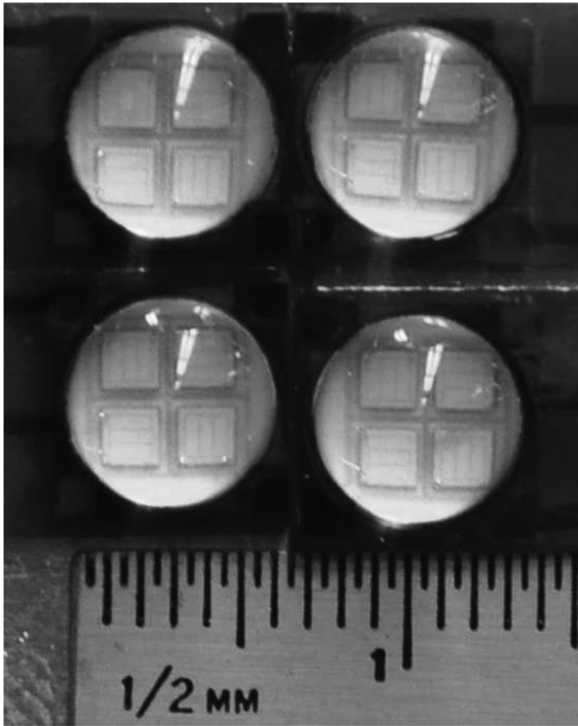
Fig. 6   Image of the 2 × 2 LED array with a scale in millimeters.

peak is reached. Laser-induced air-spark illumination [13] fails to provide the level of illumination that is required for the focusing schlieren optical system. LEDs, on the other hand, have been shown to pulse in the microsecond range or faster with the desired square-wave illumination profile [14]. The key question is whether an LED source can produce enough illumination for focusing schlieren image velocimetry.

An LED light source was developed using four 15 W high-power cool-white LEDs manufactured by LedEngin (purchased through Mouser Electronics, part number 897-LZ400CW15). These LEDs were found to be capable of producing a 0.5 μs illumination pulse, with rise and fall times of less than 0.05 μs. The present 2 × 2 LED array, shown in Fig. 6, was double-pulsed with an interpulse interval ranging from 1 to 2 μs. Figure 6 reveals that each LED dome contains four separate square emitters. The overall size of the 2 × 2 LED array is about 1.4 × 1.4 cm. Note that focusing schlieren optics does not require a small light source; in fact, an extended source is desirable for this purpose.

Figure 7 presents the circuit diagram for the LED-array pulse driver. For PIV illumination, the LED drive input is a pair of microsecond-range 15 V square waves with adjustable pulse widths and interpulse interval. For a broader discussion of microsecond LED pulsing circuits, see O'Hagan et al. [14].

This light source showcases some of the advantages of modern LEDs as schlieren light sources: high output of noncoherent white light, quick response time, small physical size, long lifetime, and low cost. LEDs are also easily switched between continuous and pulsed operation. White-light LED illumination of the present schlieren system yielded images that could be readily processed via background subtraction and histogram modification to reveal turbulent eddies. This is more difficult with laser illumination from separate laser heads, where heavy speckle competes with the eddies during image processing and analysis.

The quick response time of present LEDs allows their use for SIV, where brief light pulses are especially required for high-speed flows. The LED setup used here has a finite pulse duration that is varied between 0.5 and 2.0 μs for the present experiments. Blurring of turbulent structures during such pulses was found to be insignificant for the case of the boundary layers investigated here. The finite pulse rise and fall times also affect the determination of the time interval between the images in an SIV pair. For present purposes the interframe time interval was taken to be the interval between the initiation of each pulse, and was termed pulse separation. The pulse separation for the current data was not less than and typically twice the pulse duration time.

The small physical size of LEDs allows them to be combined in dense arrays to increase the overall illumination. Nonetheless, the 2 × 2 array used here is sufficient for recording high-speed schlieren images only when the schlieren image is focused directly into the camera lens instead of onto a ground-glass image plane. This causes a depth of focus penalty as described earlier. We have found that the use of a ground-glass screen in the image plane decreases the image illumination by 2–4 f stops due to light scattering. Even with a holographic rear-projection screen the illumination was still insufficient. However, referring to Fig. 6, two additional f stops of source illumination could readily be had by using a 4 × 4 rather than a 2 × 2 LED array. Future work will address this issue by way of a larger LED array, subject to the requirement that the incident light beam must be accommodated by the main imaging lens aperture A in Fig. 2.

The present parallel-light schlieren and shadowgraph imaging used the same LED drive and array, but only a single LED emitter of the 16 available was needed for system illumination.

D.   Image Capture and Processing

A Cooke pco.1600 cooled CCD camera was used to record the focusing schlieren image pairs of the supersonic boundary layer. This camera provides 1600 × 1200 pixel resolution with 14 bit pixel depth, and captures image pairs at about 15 Hz, yielding an average of 150 image pairs per wind-tunnel experiment. The large pixel range and field of view of this camera were found to improve the imaging of weak schlieren disturbances with the focusing schlieren system. The camera exposure for the first image of a pair, frame A, was deliberately set to be slightly longer than the first LED pulse duration. The exposure of the second image, frame B, was determined by the camera readout time and was typically several milliseconds. Frame A was therefore always precisely exposed, but frame B sometimes suffered areas of overexposure due to ambient light, even though the experiments were performed in a darkened laboratory.
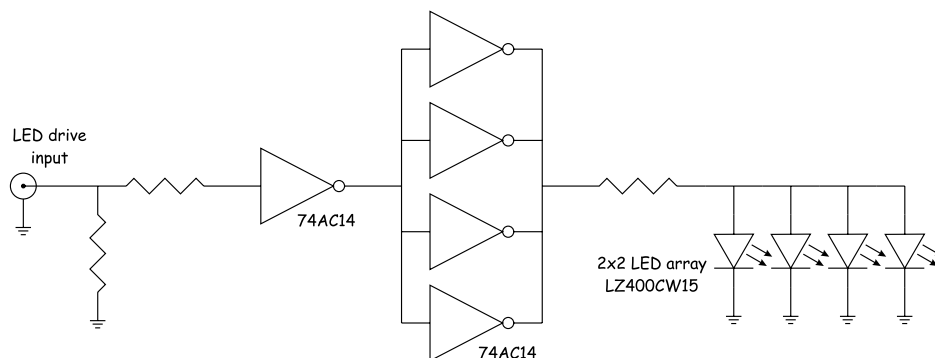

Fig. 7   Circuit diagram for the 2 × 2 LED array.

Compressible boundary-layer structures are readily visible in the focusing schlieren images recorded here, but still require image processing to improve their contrast. For each image sequence, a background image is created by averaging all images within the data set obtained during a wind-tunnel run. Different background images are determined for frames A and B. Then the common background image is subtracted from each SIV image, which is subsequently readjusted to normalized pixel values ranging between 0 (black) and 1 (white). Each image is blurred with a 3×3 pixel averaging filter to remove fine-scale nonturbulent optical noise before processing for velocimetry. A sample image pair showing both the raw and processed SIV images is given in Fig. 8. The flow is from left to right in these images, as clearly identified by the inclination of the turbulent structures.

One drawback of using a simple lens (Fig. 3) to project the focusing schlieren image into the camera lens is that some image distortion can occur. This image distortion can be seen in Fig. 8a: the flat wind-tunnel floor is clearly distorted into an arc. This image distortion can be accounted for within the SIV calibration procedure or limited by using a smaller measurement region where the distortion is not significant.

The measurement region used here is outlined in Fig. 8, and has been selected to limit the influence of image distortion on the present measurements. The SIV results are averaged in the streamwise direction over the region shown in Fig. 8. The measurement region extends from about $0.1 < y/\delta < 1.0$, as measured from a calibration image. The large SIV interrogation window required here prevented measurements of the velocity profile at heights of $y/\delta < 0.1$.

An IDT, Inc. PIV camera with 1280×1024 pixel resolution was used for the supersonic shadowgraph and schlieren visualization. The subsonic schlieren images were recorded with a TSI, Inc., 4MP camera with 2048×2048 pixel resolution. Different cameras were used throughout these experiments due to availability at the time. These cameras, in general, were all adequate for the present imaging purposes and provided sufficient pixel resolution to resolve the motion of the turbulent eddies within the schlieren images; thus, no present camera is preferred over another. All images obtained were image-processed as stated above to enhance the appearance of the turbulent structures and to improve the SIV processing.

E.   Schlieren Image Velocimetry Processing

A range of SIV processing techniques was used in the analysis of the schlieren image pairs. Commercial PIV software from IDT and
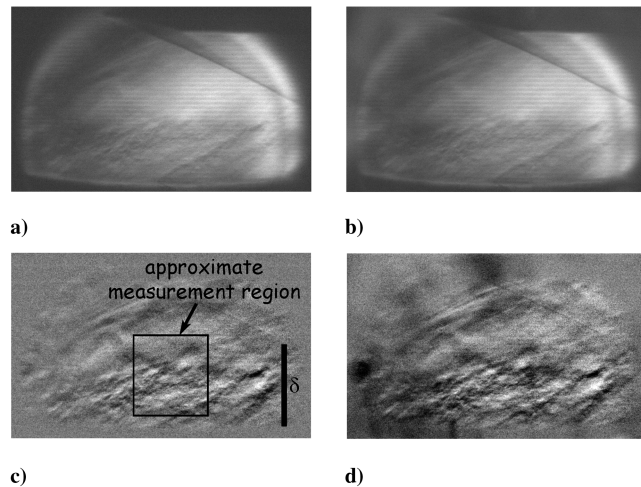
Fig. 8   Focusing schlieren images of the $M = 3$ tunnel-floor boundary layer used for SIV: a) original first image of an SIV image pair, b) second image of the image pair, c) appearance of the first image after image processing, with the measurement region and physical scale identified, d) appearance of the second image after image processing. Also visible at the tops of the images is a conical probe in the freestream and its associated oblique shock wave; the probe is present for alignment purposes only and does not affect the present measurements.

TSI were both used with limited success, whereas a custom code written in MATLAB was found to be preferable for schlieren image velocimetry processing.

The commercial software packages yielded only limited success, because schlieren images are far from being ideal PIV images. Most commercial PIV packages are written to correlate relatively small interrogation windows (tens of pixels in area), containing approximately 3–5 high-contrast, clearly defined particles on a uniform background field. Schlieren images (and especially focusing schlieren images) of turbulent structures contain large (hundreds of pixels in area) structures with widely varying grayscale texture, many having ill-defined edges. Because these structures are so large and are poorly defined, commercial software packages have trouble capturing their motion between frames, even though it can clearly be observed by the user.

A simple manual PIV analysis can be performed on these images by identifying a turbulent structure in two successive frames by eye and manually extracting the pixel shift directly from the images, as was done by Papamoschou [4,5]. Although this process can be accurate, it is also time-consuming and prone to subjective human-estimation error. Manual PIV, however, is recommended as a benchmark for any computerized analysis of schlieren images and as a reality check on the results obtained.

A more thorough analysis of the schlieren image velocimetry results was performed using a custom-written MATLAB program. This program used the standard MATLAB function `normxcorr2` to obtain a normalized cross-correlation between an identified interrogation window and a second image [15,16]. The remainder of the program is primarily bookkeeping to select a region within an image as an interrogation window and a neighborhood region in the second image to find the given structure. The function `normxcorr2` returns an array that contains the correlation coefficients for locating the interrogation window within the neighborhood region, where the maximum value within the array is the location of best correlation. The array indices for the maximum correlation coefficient are used to determine the pixel shift between images. The function `normxcorr2` thus only provides integer values of pixel shift. Image pairs with larger interframe times (and thus larger pixel shifts) are thus used here to obtain better results, higher measurement resolution, and lower uncertainties. Subpixel measurement resolution could be obtained by interpolating pixel values to create effectively larger images and then performing the correlation. Subpixel measurement resolution was found to not enhance the present results, because each sample set included 150–200 image pairs; thus, sufficient statistics were available so that additional image resolution was not required.

Table 1 provides a summary of the experiments performed here, including the SIV analysis methods and interrogation-window sizes. Comparisons made here between processing methods were made for results produced with the same size interrogation windows. The SIV analysis was performed with a 50% overlap between interrogation windows. The interrogation-window sizes were selected so that a typical turbulent eddy within the image would be fully encompassed within the interrogation window, as shown in Fig. 5. The interrogation windows were either square or rectangular, with the longer dimension in the streamwise direction, in order to improve correlations for the streamwise advection of the turbulent structures.

III.   Experimental Results and Discussion

A.   Turbulent Boundary-Layer Intermittency

An important factor in schlieren image velocimetry is turbulent intermittency. Intermittency implies that turbulent structures and essentially laminar flow regions from the freestream coexist heterogeneously within the outer part of the boundary layer. The mass-averaged velocity in an intermittent region can be inferred from mean pitot-pressure surveys, but such a low-turbulence region is problematic for SIV, because the lack of turbulent structures is analogous to a lack of PIV particles. Thus, in the intermittent regions of a turbulent flow, SIV suffers from a problem similar to inadequate seeding in traditional PIV. Understanding the intermittency in the

Table 1 Summary of experiments and SIV processing parameters

Boundary layer	Optical system	Exposure time, μs	Interframe time, μs	SIV processing software	SIV interrogation-window size, pixels
Mach 3	Focusing schlieren	0.5	1	IDT and TSI	80×50
Mach 3	Focusing schlieren	0.5	1	MATLAB	80×50
Mach 3	Schlieren	1	2	MATLAB	24×24
Mach 3	Shadowgraph	1	2	MATLAB	24×24
Subsonic (thermally seeded)	Schlieren	4	30	MATLAB	140×80

measurement region is therefore essential to the interpretation of SIV results.

The intermittency function, γ, for an incompressible turbulent boundary layer was defined by Klebanoff [17] as a function of height within the boundary layer, y/δ:

$$\gamma = \tfrac{1}{2}(1 - \mathrm{erf}\,\zeta) \qquad (3)$$

where

$$\zeta = \left(\sqrt{2}\frac{\sigma}{\delta}\right)^{-1}\left(\frac{y}{\delta} - 0.78\right) \qquad (4)$$

and the standard deviation σ is defined as

$$\sigma = 0.14\delta \qquad (5)$$

Thus defined, the intermittency function varies from 1, indicating that turbulent structures are always present, to 0 where no structures exist, as plotted in Fig. 9. From this function, an effective edge of the turbulent boundary layer can be approximated at a mean height of $y/\delta \approx 0.78$. This height represents the location where structures are present approximately 50% of the time. This approximation also indicates that the instantaneous boundary-layer edge essentially never extends outside the region $0.4 < y/\delta < 1.2$.

The ability to perform accurate SIV measurements is restricted to regions of the flow where at least some turbulent structures are present; therefore, it is expected that SIV results will progressively fail in the turbulent boundary layer (compared with the pitot-survey benchmark) when $y/\delta > 0.4$. Although this approximation is for an incompressible turbulent boundary layer, the turbulent structure of the present Mach 3 boundary layer is expected to be very similar to the incompressible case, as first suggested by Morkovin and reported by Spina et al. [12].
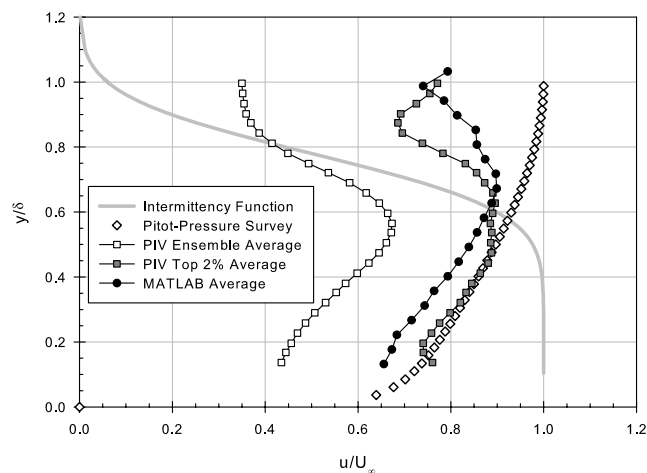

Fig. 9 Mach 3 boundary-layer mean velocity-profile data measured with pitot-pressure survey and focusing schlieren image velocimetry, also showing turbulent boundary-layer intermittency function.

B. $M = 3$ Supersonic Turbulent Boundary Layer

1. Focusing Schlieren Image Velocimetry Results

Figure 9 presents the results obtained for the boundary-layer convective-velocity profile as determined from focusing schlieren image velocimetry alongside the benchmark pitot-pressure survey result obtained by Garg and Settles [11]. Figure 9 shows the calculated boundary-layer velocity profile for PIV processing using commercially available software (PIV ensemble average) and for the MATLAB program written for this analysis (MATLAB average).

The first observation from Fig. 9 is that the commercial PIV software calculates an average velocity that is significantly lower than the measured pitot-survey result. The focusing schlieren images of the turbulent structures were typically of low contrast and lacked sufficient fine-scale turbulence to allow the commercial PIV algorithm to correlate properly. Instead, the algorithm sometimes correlated on nondescript regions or noise, resulting in nonphysical, artificially low velocities that were nonetheless included in a standard ensemble average. If these low velocities are removed, by considering only the highest 2% of measured velocities (PIV top 2% average), then the resulting velocity profile approaches the established pitot-survey benchmark for $y/\delta < 0.6$. However, this technique of isolating only the largest velocities requires a priori knowledge of the flowfield and is imprecise due to ambiguity associated with which structures the PIV software is actually correlating. On the other hand, note that it is unphysical to expect eddy velocities higher than the local convective velocity, thus considering only the fastest data has some justification.

For $y/\delta > 0.6$ the focusing schlieren image velocimetry results deteriorate quickly, even when only the maximum velocity correlations are accepted. The turbulent structures in this region are sparse, of low contrast, and significantly larger than is appropriate for analysis with the present PIV algorithm. The structures in this region can, however, be tracked through manual PIV [4,5].

When the same images are processed with the present MATLAB program using the `normxcorr2` function, the average velocity-profile result is significantly improved and more nearly approaches the pitot-survey benchmark, compared with the PIV average velocity profile. The improved results are obtained throughout the boundary layer, but the characteristic decreasing velocity at large y/δ due to intermittency remains, indicating a failure of the correlation. The MATLAB program likely has improved results because it employs a simple correlation procedure using both spatial and frequency domains to find the best correlation for the interrogation window; there are no built-in assumptions about the appearance of the PIV image, such as the expectation of high-contrast white particles on a black background.

The commercial PIV software packages produced statistically low velocity distributions for all the imaging techniques used here. The MATLAB correlation routine, on the other hand, worked well for all of the imaging techniques, returning velocity distributions which were confirmed by limited manual PIV measurements. Therefore, only these results are presented for the remainder of the present work.

2. Schlieren and Shadowgraph Results

Parallel-light schlieren and shadowgraphy, described earlier, provide several advantages over focusing schlieren for SIV analysis of two-dimensional turbulent flows: the resolution of smaller-scale structures, improved sensitivity, improved contrast, and reduced
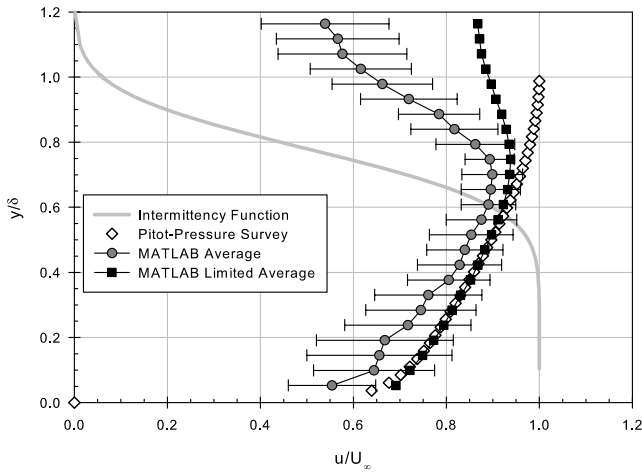
Fig. 10   Mach 3 mean boundary-layer velocity-profile data measured with pitot-pressure survey and SIV, also showing turbulent boundary-layer intermittency function. The error bars represent the standard deviation of the average and are approximately the same for the schlieren and shadowgraph measurements.

Fig. 12   Mach 3 mean boundary-layer velocity-profile data measured with pitot-pressure survey and schlieren PIV techniques, plotted in wall-wake coordinates. The boundary-layer edge is at $y+ \approx 7900$.

influence of intermittency. As presented in Fig. 5, the schlieren beam integrates across the entire test section and reveals an integrated view of many small-scale, high-contrast turbulent structures dispersed throughout the boundary layer. The intermittency also influences the results less due to integration across the test-section width, providing more structures for correlation in the outer part of the boundary layer. Since the flowfield is approximately two-dimensional, including schlieren disturbances from the sidewall boundary layers and corners in the integrated image has little influence on the results.

Figure 10 shows velocity profiles for the supersonic boundary layer as obtained by processing parallel-light images through the present MATLAB program. The MATLAB average profile presented in Fig. 10 is the average velocity profile calculated by the program, with no limits placed upon the allowable pixel shifts. The error bar shown for this measurement represents a 10–20% deviation from the mean.

Spurious correlations were next eliminated by applying Chauvenet's criterion [18], thus allowing the elimination of data outside of 2 standard deviations from the mean. Once these limits were applied (dropping approximately 15% of the original data), the MATLAB limited average velocity profile was obtained. The average velocity for $y/\delta > 0.6$ is still influenced by the intermittency, but

below that level the agreement of SIV with the pitot-survey benchmark is good.

Figure 11 shows the final boundary-layer velocity profile results from the schlieren, shadowgraph, and focusing schlieren velocimetry of the supersonic boundary layer with the average-limited MATLAB PIV analysis. The same data are also shown in Fig. 12 in wall-wake coordinates.

In general, these results show excellent agreement with the pitot-survey measurements. The focusing schlieren results show a slightly slower convective velocity and a relatively larger standard deviation on average when compared with the shadowgraph and schlieren results. The reason for the difference between the measurements is unknown, although it is likely due to the turbulent structure appearance in the focusing schlieren images causing a degraded correlation, as evidenced by the larger error bar. The focusing schlieren data is also highly susceptible to the intermittency.

Figure 12 shows that the schlieren and shadowgraph measurements accurately capture the mean turbulent boundary-layer velocity profile throughout the log-law region and partially into the wake region of the boundary layer. Future investigations will explore the near-wall region more thoroughly in order to measure the eddy velocity at smaller $y+$ values. In this study, schlieren PIV data below $y+ \approx 400$ were prevented by optical problems in the proximity of the wall.
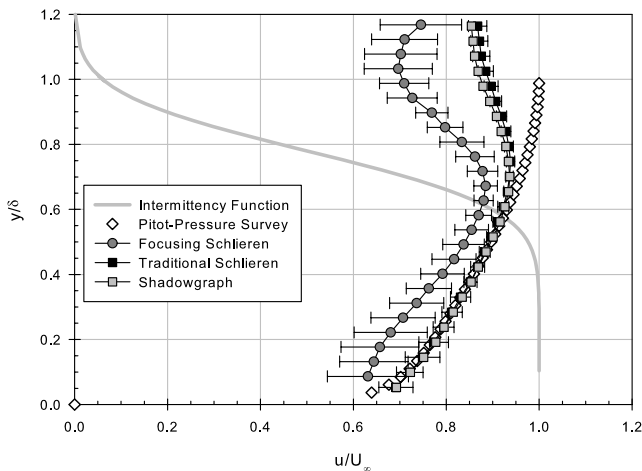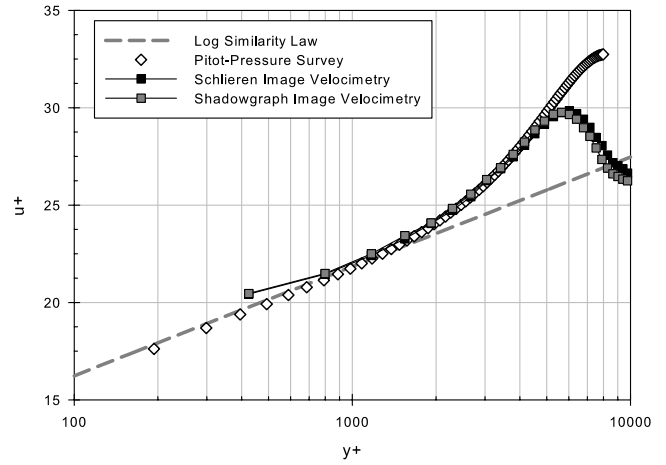

Fig. 11   Mach 3 mean boundary-layer velocity-profile data measured with pitot-pressure survey and SIV techniques, processed with the MATLAB program. The error bars represent the standard deviation of the average and are approximately the same for the schlieren and shadowgraph measurements.
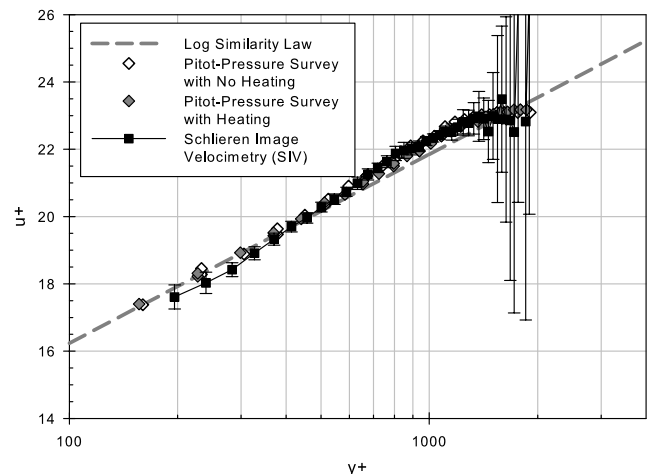

Fig. 13   Mean subsonic boundary-layer velocity-profile data measured with pitot-pressure survey and SIV, processed with the MATLAB program. The boundary-layer edge is at $y+ \approx 1430$. The error bars represent 1 standard deviation from the mean on the SIV results.

C. Subsonic Turbulent Boundary Layer

Figure 13 presents the schlieren velocimetry measurements made in the thermally seeded subsonic turbulent boundary layer. The SIV data agree well with the pitot survey, except in the region of $y +$ <400 where the SIV measurements show a slightly lower mean velocity. At the boundary-layer edge the average velocity is accurately captured, although with a significant error bar. These data more accurately capture the velocity near the freestream, because the tunnel test section is significantly wider (width $\sim 20\delta$) than the supersonic test section (width $\sim 6\delta$), and thus the integrating optics are less affected by intermittency. Also the freestream is utterly clear of refraction, so the motion correlation acts only upon real eddies near the boundary-layer edge. The large error in this region is still a result of intermittency, however. Note that the subsonic turbulent boundary layer has very little wake component, and that the pitot-survey results with and without heating show little effect of heating on the mean velocity profile.

IV. Conclusions

Schlieren image velocimetry (SIV) is a potentially useful seedless-velocimetry technique that is capable of performing velocimetry measurements using naturally occurring turbulent eddies within a flow as PIV "particles." SIV techniques have been demonstrated with a range of optical systems and applications including both compressible and incompressible flows. These techniques can be directly applied to any turbulent flow containing refractive-index gradients. Turbulent compressible flows contain naturally occurring density gradients within the turbulent eddies that can be used for this purpose. To apply this technique to incompressible flows a refractive disturbance must be created within the flow using either temperature or chemical species seeding, as is done here by heating the boundary layer. The SIV technique uses turbulent structures as particles and thus cannot be directly applied to laminar flows or to flows with significant turbulent intermittency.

The velocity measurements from schlieren, shadowgraph, and focusing schlieren imaging techniques in a $M = 3$ compressible turbulent boundary layer were compared with results derived from a pitot-pressure survey profile of a compressible turbulent boundary layer on the floor of the PSGDL's supersonic wind tunnel. Reasonable agreement was demonstrated with the pitot-survey benchmark. The ability to perform accurate schlieren and shadowgraph image velocimetry measurements in this turbulent flow, however, is limited by the inherent intermittency of the turbulent boundary layer. Because these SIV techniques rely on turbulent structures as particles, the intermittent low-turbulence regions near the boundary-layer edge currently preclude the ability to perform accurate turnkey PIV measurements of the entire mean convective-velocity profile.

Present commercial PIV software packages do not perform well when processing schlieren images. This is due to the large, nondistinct, low-contrast appearance of the turbulent structures. Commercial algorithms are not designed for such images and therefore should not be used for schlieren image velocimetry. A simple MATLAB program, however, using the function `normxcorr2`, produces accurate results. Before any form of PIV processing, image processing should be performed on the images to remove artifacts through an average image subtraction and to enhance contrast through a histogram stretch.

Focusing schlieren, with a limited depth of focus, provides seedless velocimetry within a restricted depth of field. Focusing schlieren velocimetry, however, is highly susceptible to turbulent intermittency. Its results should be compared with other measurements from probes or integrating SIV results to build confidence in the measurement. As the depth of focus decreases, schlieren sensitivity, image contrast, and the frequency of turbulent eddies also decrease, while the apparent eddy feature size increases, thus hindering the ability to accurately determine velocity magnitude from SIV. For the present system, with a depth of focus of approximately ± 40 mm, boundary-layer images can be obtained that contain sufficient contrast and eddy density to perform an accurate SIV analysis with a custom-written correlation code.

Schlieren and shadowgraphy with parallel light typically result in higher-contrast and feature-dense images that are more suitable for SIV analysis. The integration along the optical path produces path-averaged velocity measurements, but can still be appropriate for nearly two-dimensional flowfields such as the present compressible and incompressible boundary layers. The increased feature density results in improved correlations throughout the boundary layer, including measurements in the intermittent regions and near the freestream. These velocimetry techniques also have the potential to measure unsteady-flow parameters such as the rms velocity, turbulence intensity, probability distribution function, etc. Although this was beyond the present scope, it is important for future study.

Although intermittency influences the current results, it remains primarily a data-processing-related issue. An improved PIV algorithm, with considerations of schlieren images containing intermittent and low-contrast regions, would be an important step toward the ability to analyze a flow by schlieren image velocimetry with no a priori knowledge of the flow characteristics.

LEDs were used as the light sources for the present imaging systems and show significant advantages over conventional laser illumination. The LED light array developed here produced high-output noncoherent light that allowed resulting schlieren and shadow images to be postprocessed, whereas this postprocessing was difficult or impossible with coherent laser illumination. The LEDs are also compact, allowing the creation of LED arrays for use in a range of visualization systems. The use of a finite LED light pulse did not limit the ability to perform the present measurements, although the pulse duration should be independently evaluated for a given flowfield application.

References

[1] Raffel, M., Willert, C. E., and Kompenhans, J., *Particle Image Velocimetry*, 3rd ed., Springer, New York, 1998.

[2] Jonassen, D. R., Settles, G. S., and Tronosky, M. D., "Schlieren 'PIV' for Turbulent Flows," *Optics and Lasers in Engineering*, Vol. 44, Nos. 3–4, 2006, pp. 190–207.
doi:10.1016/j.optlaseng.2005.04.004

[3] Townend, H., "A Method of Airflow Cinematography Capable of Quantitative Analysis," *Journal of the Aeronautical Sciences*, Vol. 3, 1936, pp. 343–352.

[4] Papamoschou, D., "A 2-Spark Schlieren System for Very-High Velocity-Measurement," *Experiments in Fluids*, Vol. 7, No. 5, 1989, pp. 354–356.
doi:10.1007/BF00198454

[5] Papamoschou, D., "Structure of the Compressible Turbulent Shear-Layer," *AIAA Journal*, Vol. 29, No. 5, 1991, pp. 680–681.
doi:10.2514/3.59935

[6] Fu, S., and Wu, Y., "Detection of Velocity Distribution of a Flow Field Using Sequences of Schlieren Images," *Optical Engineering*, Vol. 40, No. 8, 2001, pp. 1661–1666.
doi:10.1117/1.1386792

[7] Settles, G. S., *Schlieren and Shadowgraph Techniques: Visualizing Phenomena in Transparent Media*, Springer-Verlag, Berlin, 2001.

[8] Schardin, H., "Die Schlierenverfahren und Ihre Anwendungen," *Ergebnisse der Exakten Naturwissenschaften*, Vol. 20, 1942, pp. 303–439.
doi:10.1007/BFb0111981

[9] Weinstein, L., "Large-Field High-Brightness Focusing Schlieren System," *AIAA Journal*, Vol. 31, 1993, pp. 1225–1250.

[10] Alvi, F. S., Settles, G. S., and Weinstein, L. M., "A Sharp-Focusing Schlieren Optical Deflectometer," AIAA Aerospace Sciences Meeting and Exhibit, Reno, NV, Jan. 1993, AIAA Paper 93-0629, 1993.

[11] Garg, S., and Settles, G. S., "Measurements of a Supersonic Turbulent Boundary Layer by Focusing Schlieren Deflectometry," *Experiments in Fluids*, Vol. 25, No. 3, 1998, pp. 254–264.
doi:10.1007/s003480050228

[12] Spina, E., Smits, A., and Robinson, S., "The Physics of Supersonic Turbulent Boundary-Layers," *Annual Review of Fluid Mechanics*, Vol. 26, 1994, pp. 287–319.
doi:10.1146/annurev.fl.26.010194.001443

[13] Volpe, J. A., and Settles, G. S., "Laser-Induced Gas Breakdown as a Light Source for Schlieren and Shadowgraph Particle Image Velocimetry," *Optical Engineering*, Vol. 45, No. 8, 2006, Paper 080509.
doi:10.1117/1.2332867

[14] O'Hagan, W., McKenna, M., Sherrington, D., Rolinski, O., and Birch, D., "MHz LED Source for Nanosecond Fluorescence Sensing," *Measurement Science and Technology*, Vol. 13, 2002, pp. 84–91.
doi:10.1088/0957-0233/13/1/311

[15] "MATLAB User Manual," MathWorks, Inc., Natick, MA, 2008.

[16] Lewis, J. P., "Fast Normalized Cross-Correlation," *Vision Interface*, Canadian Image Processing and Pattern Recognition Society, 1995.

[17] Klebanoff, P. S., "Characteristics of Turbulence in a Boundary Layer with Zero Pressure Gradient," NACA TR 1247, 1955.

[18] Taylor, J. R., *An Introduction to Error Analysis*, 2nd ed., University Science Books, Sausalito, CA, 1997.

R. Lucht
Associate Editor